JOC The Journal of Organic Chemistry

Article

Water Soluble NIR Absorbing and Emitting Indolizine Cyanine and Indolizine Squaraine Dyes for Biological Imaging

William E. Meador, Shane A. Autry, Riley N Bessetti, Jacqueline N. Gayton, Alex S Flynt, Nathan I Hammer, and Jared H. Delcamp

J. Org. Chem., **Just Accepted Manuscript** • DOI: 10.1021/acs.joc.9b03108 • Publication Date (Web): 10 Feb 2020

Just Accepted

is published by the American Chemical Society. 1155 Sixteenth Street N.W., Washington, DC 20036

Water Soluble NIR Absorbing and Emitting Indolizine Cyanine and Indolizine Squaraine Dyes for Biological Imaging

William E. Meador,[a] Shane A. Autry,[a] Riley N. Bessetti,[b] Jacqueline N. Gayton,[a] Alex S. Flynt,[b] Nathan I. Hammer,[a] and Jared H. Delcamp[a,*]

[a]Department of Chemistry and Biochemistry, University of Mississippi, University, MS, 38677
[b]Department of Biological Sciences, University of Southern Mississippi, Hattiesburg, MS, 39406

email: delcamp@olemiss.edu

Abstract

Organic dyes that absorb and emit in the near infrared region are potentially non-invasive, high resolution, and rapid biological imaging materials. Indolizine donor-based cyanine and squaraine dyes with water solubilizing sulfonate groups were targeted in this study due to strong absorptions and emissions in the NIR region. As previously observed for non-water soluble derivatives, the indolizine group with water solubilizing groups retains a substantial shift toward longer wavelengths for both absorption and emission with squaraines and cyanines relative to classically researched indoline donor analogues. Very high quantum yields (as much as 58%) have been observed with absorption and emission >700 nm in fetal bovine serum. Photostability studies, cell culture cytotoxicity, and cell uptake specificity profiles were all studied for these dyes, demonstrating exceptional biological imaging suitability.

Abstract Image

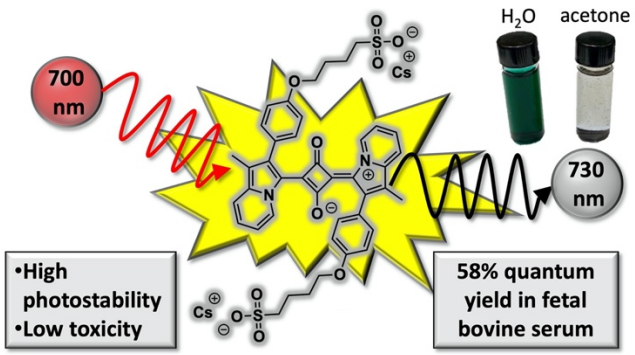

Introduction

Near-infrared (NIR) emissive materials are intensely researched due to a plentiful number of practical applications including biological imaging,[1-8] photodynamic therapy,[1, 9-12] telecommunications,[13-15] secure displays which can be coupled to night vision technologies,[16-18] and many other innovative areas of research.[5, 19-21] NIR biological imaging agents use low energy photons in a spectral region where tissue is readily penetrated at a maximal depth optically.[4, 10, 22-23] Desirable properties of biological imaging dyes include: 1) absorbing and emitting light in the "therapeutic window" ranging from 700-1400 nm, 2) a significant Stokes shift to enable high-precision imaging, 3) efficient absorption and emission of photons through both a high molar absorptivity and quantum yield, and 4) water solubility. While there are many exciting dye design prospects being pursued in the literature,[2] exceptional NIR emissive materials are still needed for practical biological imaging since current dyes fall short of meeting all of the desired criteria simultaneously.

Among NIR emissive dyes, squaraines[21, 24] and cyanines[19, 25] are ubiquitous.[1, 3, 26] Previous research has frequently investigated indoline donor-based cyanine and squaraine dyes with indocyanine green (ICG) having been awarded FDA approval several decades ago.[27-28] Both of these classes of dyes need design strategies that allow access to longer wavelength NIR photons in aqueous environments.[2] In fact, the indoline squaraine absorbs outside the therapeutic window which renders it impractical for use as a non-invasive biological imaging agent.[29] To deepen the NIR absorbing properties of these dye classes, designs capable of extending the π-system through a conjugated donor (such as indolizine) are attractive.[29-32] Recent photophysical studies using proaromatic indolizine donors in place of indoline donors show red-shifting of the absorption and emission profiles of these dyes firmly into the therapeutic window in non-aqueous environments (**C5** and **SQ** compared to ICG and indoline squaraine, respectively; Figure 1).[29-32] These studies indicated that in the case of phenyl-indolizine derivatives, the phenyl group does not play a significant role in tuning the absorption or emission energy values of the NIR indolizine dyes.[29-30] This enables the use of the phenyl group to append water soluble functionality without perturbing the core chromophore properties of the dyes, permitting the probing of the photophysical properties of the dyes in aqueous environments. Sulfonate substituted dyes, **SO_3C5** and **SO_3SQ**, were targeted given the water solubilizing properties of sulfonate groups and example FDA

approval for human use by way of ICG (Figure 1). This work aims to compare the photophysical properties of **SO_3C5**, **SO_3SQ**, and benchmark ICG in biologically relevant medium.

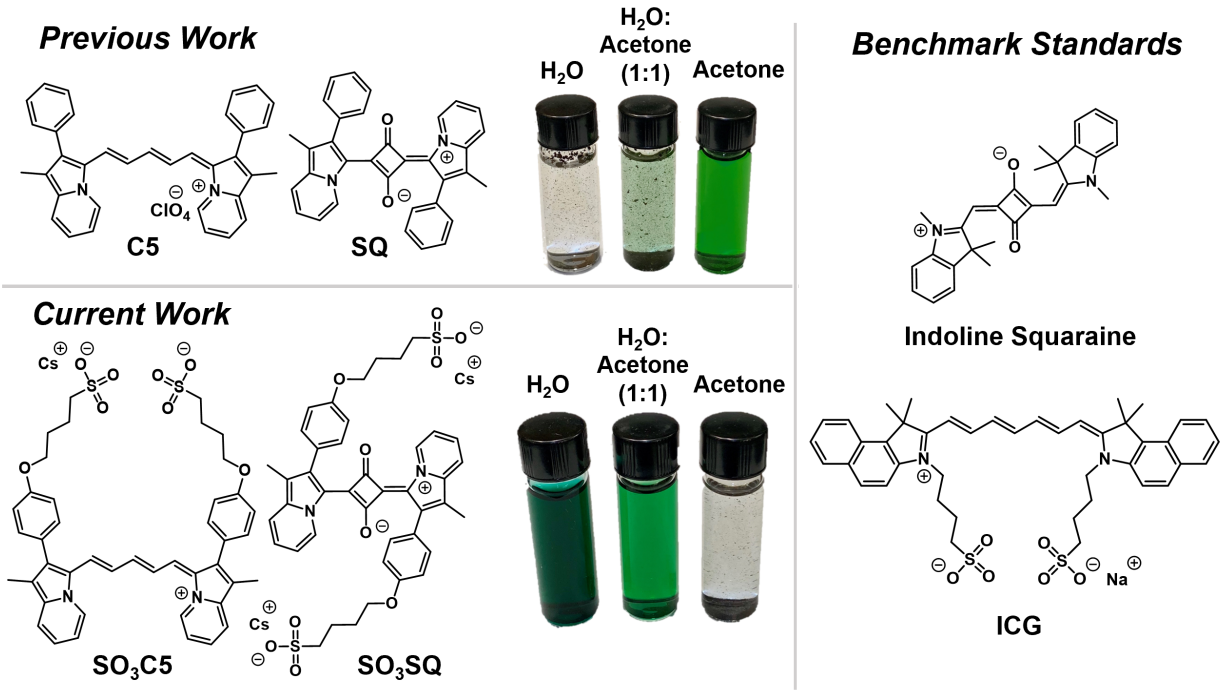

Figure 1. Current work demonstrating water solubility of indolizine cyanine and indolizine squaraine dyes using sulfonate groups.

Synthesis

The target dyes were synthesized in 2-steps from previously reported indolizine phenol **1** (Scheme 1).[29] First, **1** was alkylated with butane sultone (**2**) in the presence of base to give sulfonate indolizine **3**. Interestingly, this reaction required a careful selection of solvent and base to avoid significant side product formation as a carbon alkylated product (see Table S1 and Figure S1). Intermediate **3** is common to both **SO_3C5** and **SO_3SQ** target dyes. The target sulfonate-indolizine cyanine dye (**SO_3C5**) is synthesized by reacting **3** with the methine bridge linker **4** in the presence of perchloric acid and acetic anhydride at room temperature similar to previously reported conditions in the literature.[30] The target sulfonate-indolizine squaraine (**SO_3SQ**) is synthesized *via* an electrophilic aromatic substitution/condensation reaction between sulfonate indolizine **3** and the squaric acid (**5**). Importantly, during optimization of the condensation reaction it was found that addition of small amounts of water led to an *increase* in product formation.

Ultimately running the reaction in non-dried laboratory grade methanol gave the highest yields (Table S2). Both target dyes are formed in approximately 50% overall yield in this route over 2 steps.

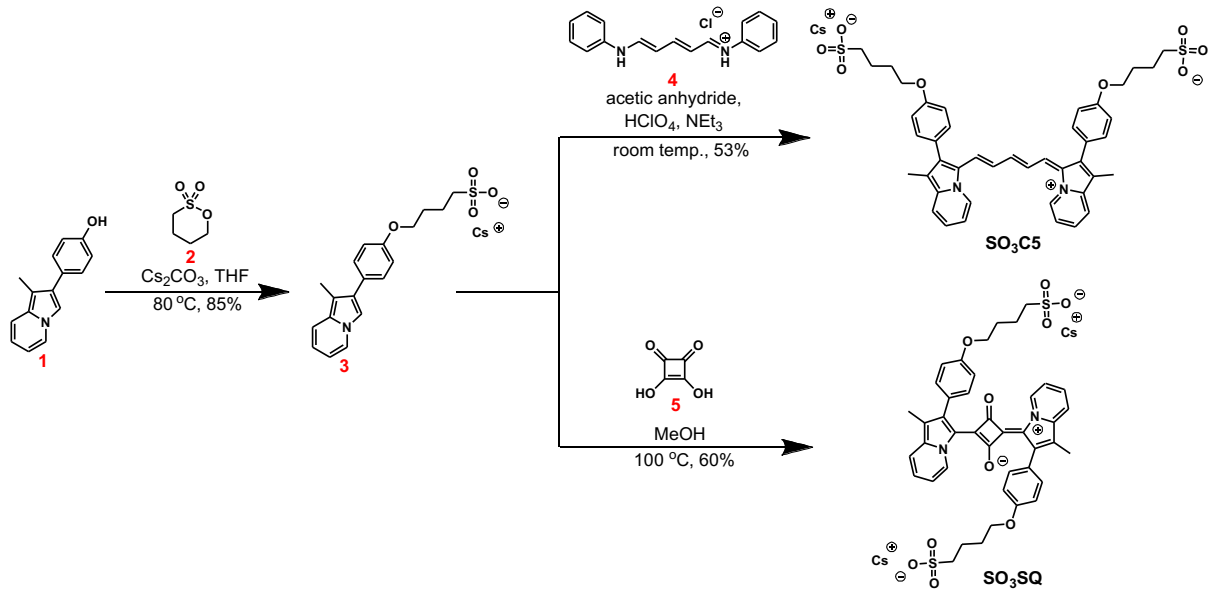

Scheme 1. Synthetic route to **SO_3C5** and **SO_3SQ**.

Results and Discussion

With **SO_3C5** and **SO_3SQ** in hand, absorption and emission studies were undertaken for comparison to ICG as a benchmark reference dye (Figures 2, S2-S3; Table 1). DMSO and MeOH were also selected as solvents which allows for the comparison of **SO_3C5** and **SO_3SQ** to the previously reported dyes **C5** and **SQ**, respectively (see Table S3 for solubility data).[29-30] H_2O and fetal bovine serum (FBS) were selected as well due to biological relevance and for a convenient analysis of how these dyes will behave with biological matrix elements in place as has been previously reported in the literature.[4, 33-34] The absorption profiles of both dyes in DMSO and MeOH are not significantly changed relative to the previously published dyes with no sulfonate groups.[29-30] The absorption curves in H_2O and FBS are similar to the curves observed in DMSO and MeOH for **SO_3SQ**; however, the absorption curve of **SO_3C5** in water deviates shape significantly which is likely due to aggregation in water (Figure S4). Upon changing concentrations no significant evidence of aggregate disruption could be observed down to concentrations near the detection limit of the spectrometer (Figure S5). Notably, evidence of

aggregation of **SO_3SQ** (modest amounts) and **ICG** (significant amounts) in H_2O at concentrations of $\geq 10^{-5}$ M is apparent at higher energy wavelengths when the absorption curves are overlaid with curves at 10^{-6} M in H_2O which appear to have disrupted aggregate features (Figures S6-S7).[35] It should be noted that while all three dyes were observed to form aggregates in H_2O *via* dynamic light scattering analysis at 5×10^{-6} M. (Figure S8), **SO_3C5** is the only dye that shows a significant impact of this aggregative behavior from the absorption profile. Interestingly, upon dissolving **SO_3C5** in FBS the original curve shape observed in DMSO and MeOH is regained with a notable red-shift of the λ_{max} value by about 40 nm (Figure 2).

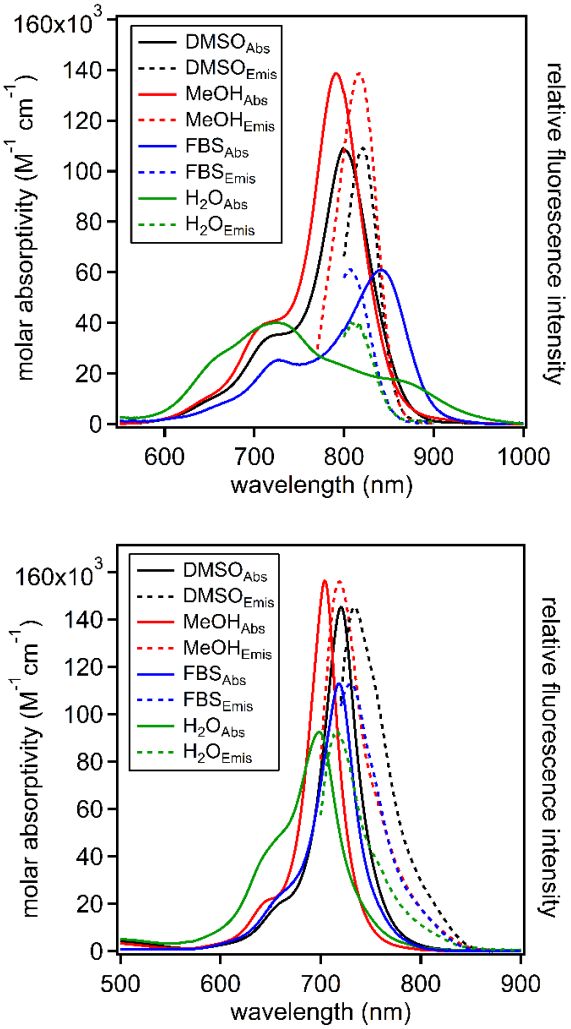

Figure 2. Vis-NIR region molar absorptivity and normalized fluorescence emission of **SO_3C5** (top) and **SO_3SQ** (bottom) in DMSO, MeOH, H_2O, and FBS at 5×10^{-6} M.

Table 1. Optical properties of **SO_3C5**, **SO_3SQ**, and ICG in water, fetal bovine serum (FBS), methanol, and DMSO.

Dye	Solvent	Abs. max. [nm]	Emis. max. [nm]	Stokes shift [nm | eV | cm^{-1}]	ε [M^{-1} cm^{-1}]	Φ [%]	MB [ε × Φ]
SO_3C5	DMSO	801	821	20 | 0.04 | 304	109,000	2.0	2,180
	MeOH	791	817	26 | 0.05 | 403	139,000	0.3	420
	FBS	842	808	---	61,000	0.1	60
	Water	726	808	---	40,000	0.05	20
SO_3SQ	DMSO	720	734	14 | 0.03 | 265	145,000	8.6	12,500
	MeOH	704	719	15 | 0.04 | 296	156,000	0.8	1,250
	FBS	719	730	11 | 0.03 | 210	113,000	58.3	65,900
	Water	698	716	18 | 0.04 | 360	93,000	0.3	280
ICG	DMSO	794	825	31 | 0.06 | 473	211,000	11.0	23,200
	MeOH	784	819	35 | 0.07 | 545	230,000	4.3	9,900
	FBS	798	827	29 | 0.05 | 439	174,000	9.3	16,200
	Water	779	812	33 | 0.06 | 522	157,000	0.5	780

FBS is commonly used in photophysical studies for NIR dyes intended for biological use as the albumin proteins help to better separate dye molecules from one another as is dramatically demonstrated here. The disruption of aggregation under biologically relevant conditions is encouraging as it leads to the minimization of thermal relaxations resulting in increased quantum yields. For comparison, the curve shape of ICG retains the same profile in all 4 solvents (Figure S3). The molar absorptivities are similar for **SO_3C5** and **SO_3SQ** in MeOH and DMSO at approximately 110,000-150,000 $M^{-1}cm^{-1}$ (Figure 2; Table 1). In H_2O and FBS, the **SO_3C5** molar absorptivities drop substantially to ~60,000 $M^{-1}cm^{-1}$ or less. For **SO_3SQ** in H_2O or FBS, the molar absorptivities remain significantly higher at 113,000-93,000 $M^{-1}cm^{-1}$. The molar absorptivity values and order of λ_{max} values follow the same trend for **SO_3SQ** and ICG with each of the four solvents. **SO_3C5** deviates from this trend with obvious aggregation in water-based solutions. Compared to ICG, the λ_{max} of **SO_3C5** is shifted toward lower energy values (~15 nm), and the λ_{max} of **SO_3SQ** is shifted toward higher energy by about 100 nm (0.21 eV, Table 1).

Fluorescence spectroscopy was probed with each of the dyes to understand the excited-state behavior. Prior reports on **C5** and **SQ** in organic solvents such as dichloromethane have shown Stokes shifts of 43 nm and 50 nm, respectively (taken as the difference between the λ_{max}^{abs} and λ_{max}^{emis}).[29-31] The Stokes shifts of both sulfonate dyes decreased to ≤26 nm (≤400 cm^{-1}) in all solvents where single molecule behavior is likely occurring. As the magnitude of the Stokes shift is directly related to the reorganization energy of the dye, the decrease in the Stokes shift demonstrates that there is a smaller reorganization energy of **SO_3SQ** and **SO_3C5** relative to the non-sulfonate substituted dyes. Stokes shifts for **SO_3C5** could not be determined in FBS and H_2O due to the presence of multiple species due to aggregation, leading to apparent emission energies higher than the lowest energy features of the combined absorption spectrum of all monomer and aggregate states. This suggests that in aqueous solvents, the higher energy absorption feature of **SO_3C5** represents the observed emission while the lower energy absorption feature is either weakly emissive or has an emission beyond the InGaAs fluorimeter detection limit.

Quantum yields (Φ) for each dye were calculated as relative values with respect to ICG in DMSO at 11.0% as the benchmarking system (Table 1).[36] The quantum yields for ICG in water, MeOH, and FBS were calculated with respect to ICG in DMSO. Previously reported quantum yields for **C5** in organic solvents ranged from 2-3.6%;[30-31] however, **SO_3C5** shows Φ values below 1% in all three protic solvents examined. In DMSO, a Φ of 2% is observed which is similar to the values observed for the parent **C5** structure. The Φ data for **SO_3SQ** is exceptionally intriguing. In water or methanol, the Φ of **SO_3SQ** is <1% which is not uncommon in the NIR spectral region. Upon changing the solvent environment to DMSO a significantly increased Φ value of 8.6% is observed, which can be rationalized as the protic environments promoting non-radiative decay pathways leading to low Φ values in water and methanol. However, **SO_3SQ** in FBS gives a 58% quantum yield, which is a number that is truly remarkable in the field of NIR dyes and encourages further studies with this material. The dramatic enhancement of Φ values in the complex biologically relevant environment of FBS has been previously observed in the literature.[33] By comparison, the benchmark dye ICG shows a much lower 9% Φ in FBS.

An important metric for biological imaging materials is the molecular brightness (MB) which balances the contributions of ε and Φ through the equation MB = ε × Φ. MB is a good indicator of the amount of dye needed to give comparable fluorescence signal intensities among

dyes with varying molar absorptivities and quantum yields. The MB values for **SO_3C5** are quite low in all solvents at ≤ 2,180 $M^{-1}cm^{-1}$ when compared with ICG at a maximum value of 23,000 $M^{-1}cm^{-1}$ in DMSO (Table 1). Notably, the observed MB value for ICG is low in H_2O at 780 $M^{-1}cm^{-1}$, but remains high in the remaining solvents examined (>9,000 $M^{-1}cm^{-1}$). **SO_3SQ** shows a MB value of >65,000 $M^{-1}cm^{-1}$ in FBS which is dramatically larger than the substantial 23,000 $M^{-1}cm^{-1}$ value for ICG and is likely one of the largest values in this spectral region known in the literature. This indicates significantly less dye (~3× less) would be needed with **SO_3SQ** to generate the same amount of signal as ICG.

A key desirable property of biological imaging dyes is prolonged photostability.[37] To probe this, **SO_3C5**, **SO_3SQ**, and ICG were dissolved in water under ambient atmosphere at a concentration of 1 x 10^{-6} M and irradiated with a solar simulated LED spectrum from 400 nm to 1100 nm with white light irradiation (Figures 3, S9-S11). Under these conditions ICG has a half-life of approximately 35 minutes with complete consumption by 80 minutes. Both **SO_3C5** and **SO_3SQ** show a higher photostability than ICG with half-lives of 50 minutes and 100 minutes, respectively. The higher photostability of **SO_3SQ** can be attributed in part to the squaraine structure being devoid of double substituted alkenes which are known to undergo various degradation pathways with ICG.[38] In MeOH, **SO_3SQ** and ICG are exceptionally stable with half-lives >24 hours (Figures S12-S15). **SO_3C5** is notably less stable than ICG or **SO_3SQ** in MeOH where the dye appears to be deaggregated, which suggests the aggregate states of **SO_3C5** in water could impart some photostability since this dye is more stable than ICG in water. Overall, **SO_3SQ** has a

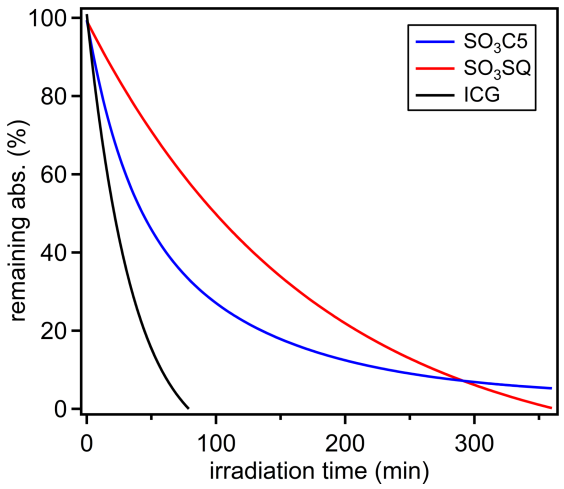

Figure 3. Photostability of **SO_3C5**, **SO_3SQ**, and ICG in water.

likely record quantum yield in this spectral region, a high molar absorptivity, an exceptional molecular brightness, and the highest photostability measured in this study in H_2O.

Finally, the cytotoxicity and cellular uptake of **SO_3C5** and **SO_3SQ** was examined with human (HEK293) and *Drosophila* (S2) tissue culture cells (Figure 4). Dyes were tested in two cell lines: HEK293 and *Drosophila* (S2). HEK cells are a human cell line grown at physiological conditions found in mammals. Performance and cytotoxicity of the dyes in HEK cells informs in vivo biocompatibility for clinical and veterinary settings for use in diagnostic or therapeutic technologies. In contrast, S2 cells grow at lower temperature under normal atmospheric conditions and are derived from invertebrates (fruit fly embryos). Dye behavior in these cells is a proxy for understanding the environmental impact of these compounds. Both **SO_3C5** and **SO_3SQ** show <25% HEK cell death at or below 2 mM concentrations. At high dye loadings (10 mM), cell death is near 30%, which indicates that these dyes are relatively benign toward a human cell line. A similar trend is observed with the cytotoxicity studies of the S2 cell line, although ≥2 mM **SO_3C5** and 10 mM **SO_3SQ** show >50% cell death. S2 cells are more phagocytically active compared to HEK293s, which may explain greater sensitivity to the dyes. This suggests that low to moderate concentrations of the dyes are not toxic to animal cells. **SO_3C5** and **SO_3SQ** cell uptake studies were undertaken with LysoTracker® by comparing fluorescence overlap of each NIR dye with LysoTracker®. With these studies, the **SO_3C5** dye shows a Pearson's correlation coefficient of 0.9 indicating HEK cells largely uptake this dye into the cell lysosomes. A similarly high Pearson's correlation coefficient is observed for **SO_3SQ** and S2 cells at 0.7. This shows that non-favorable interactions of the dye with cell organelles is minimized.

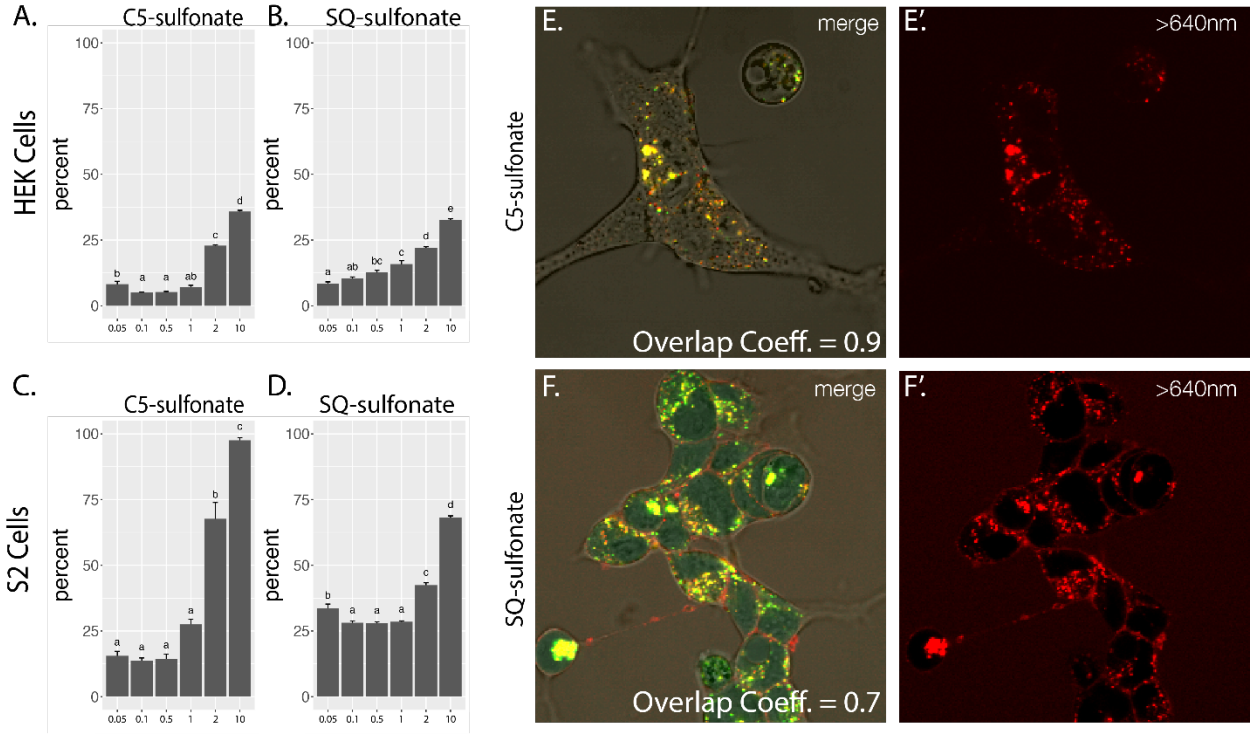

Figure 4. Interaction of **SO_3C5** and **SO_3SQ** dyes with human (HEK) and *Drosophila* (S2) cells. A-D) Percent cytotoxicity for each combination as determined by LDH assay. X-axis values are mM. Error bars represent standard error, and letter denote significance groups determined by TukeyHSD ($p \leq 0.05$). E-F) Confocal images of live HEK (E) and S2 (F) cells after exposure to dye and LysoTracker®. Left panels are merge of bright field, lysotracker (green), and dye (red). Dye fluorescence alone is right (E',F'). Pearson's correlation coefficient (noted as the overlap coefficient) shows colocalization between dye and LysoTracker®.

Conclusion

The need for biological imaging dyes that absorb and emit strongly in the NIR region is of paramount importance to society since this could enable non-invasive, non-toxic, and rapid imaging of medical patients and biological specimen. Indolizine donor-based cyanine and squaraine dyes with attached sulfonate groups were synthesized to provide a direct comparison in biological medium to benchmark ICG. The increased donor strength of the indolizine compared to that of the indoline allowed for these dyes to have a more red-shifted absorption and emission than their indoline counterparts. **SO_3SQ** demonstrated a remarkable quantum yield of 58.3% (MB of >65,000) in FBS which is notable in that this is representative of the optical properties inside of

a biological medium. **SO_3C5** shows significant concentration independent aggregation effects in water, while **SO_3SQ** shows minimal aggregation in water. Prolonged irradiation studies demonstrate that both of the indolizine dyes have a significantly higher photostability than ICG in water. Cell culture studies exhibited high specificity for lysosomal uptake with overlap coefficients of 0.9 and 0.7 for **SO_3C5** and **SO_3SQ** respectively, as well as low levels of cytotoxicity. The high molecular brightness, simple synthesis, prolonged photostability, and low toxicity of **SO_3SQ** shows that it is an attractive potential NIR biological imaging material with very high metrics significantly surpassing the benchmark ICG over a range of tests.

Experimental Section

All commercially obtained reagents and solvents were used as received without further purification. All heating was done in an oil bath. Thin-layer chromatography (TLC) was conducted with Merck KGaA TLC Silica gel 60 RP-18 $F_{254}S$ glass backed plates and visualized with UV. Flash column chromatography was performed using a CombiFlash Rf+ system. RediSep cartridges were charged with silica gel from RediSep® Rf Reversed-phase C18, 40−63 μm (230−400 mesh). ^1H and ^{13}C $\{^1H\}$ NMR spectra were recorded on a Bruker Ascend-300 (300 MHz) spectrometer and are reported in ppm using solvent as an internal standard (DMSO-d6 at 2.50 ppm and CD_3OD-d4 at 3.31 ppm). Data are reported as s = singlet, d = doublet, t = triplet, q = quartet, p = pentet, m = multiplet, b = broad, ap = apparent, dd = doublet of doublets, dt = doublet of triplets; coupling constant(s) are in Hz; integration. UV−vis-NIR spectra were measured[13] with a Cary 5000 UV−vis−NIR spectrometer. For photostability studies, samples were irradiated with a Class AAA Rated G2V pico LED Solar Simulator providing a spectral range from 400 nm – 1,100 nm at 100 mW/cm^2. HRMS spectra were obtained with a QTOF HRMS utilizing nanospray ionization. The mass analyzer was set to the 200−2000 Da range. Infrared spectra were recorded with an Agilent Cary 660 ATR-FTIR. All emission data was obtained using a Horiba PTI fluorimeter. Excitation wavelengths were achieved by passing white light through a dual grating system. Photons were collected through a photomultiplier tube. The relative quantum yields were obtained using this equation:

$$\Phi_{sample} = \Phi_{standard} \cdot \frac{E_{sample}}{E_{standard}} \cdot \frac{A_{sample}}{A_{standard}} \cdot \frac{\eta^2_{sample}}{\eta^2_{standard}}$$

For the equation above, E is the sum of emission intensities and A is maximum absorbance. η is the refractive index of the solvent used, and Φ denotes the quantum yield. The standard used to obtain the relative quantum yields was Indocyanine Green (ICG) with a quantum yield of 11% in DMSO.[36]

Cell Imaging: HEK293 cells were grown in standard conditions (37 °C, 5% CO2) in DMEM media supplemented with 10% FBS. S2 cell cultures were maintained in S2 media with 10% FBS at 25 °C. Dye cytotoxicity was determined with a CyQUANT LDH Cytotoxicity Assay Kit™ Invitrogen using a BioTek Synergy™ H1 microplate reader. Cells were imaged with a Zeiss LSM 510 META laser scanning confocal microscope following 24 hour exposure to dyes. Lysosome were visualized with LysoTracker® Green DND-26 (Invitrogen) following manufacturer protocols.

Cesium 4-(4-(1-methylindolizin-2-yl)phenoxy)butane-1-sulfonate (**3**): To a flame dried round bottom flask equipped with a stir bar and reflux condenser that had been purged with N_2 for 10 minutes was added 4-(1-methylindolizin-2-yl)phenol (**1**) (1.00 g, 4.48 mmol),[29] Cs_2CO_3 (3.65 g, 11.20 mmol), and 1,4-butane sultone (**2**) (1.15 mL, 11.20 mmol). The reaction mixture was dissolved in THF (140 mL) and heated to 80 °C in an oil bath for 16 hours. The reaction mixture was cooled to room temperature and yielded a light brown precipitate. Ethyl acetate was added (100 mL) to further precipitate the product, which was subsequently filtered to yield the crude material. The crude was purified by recrystallization in water to yield a pure golden brown metallic in appearance solid (1.87 g, 85%). ^{1}H NMR (300 MHz, DMSO-d6, Figure S16) δ 8.13 (d, *J* = 6.9 Hz, 1H), 7.63 (s, 1H), 7.42 (d, *J* = 8.7 Hz, 2H) 7.37 (d, *J* = 9.1 Hz, 1H), 6.99 (d, *J* = 8.7 Hz, 2H), 6.60 (dd, *J* = 8.1 Hz, 7.2 Hz, 1H), 6.45 (dt, *J* = 7.1 Hz, 1.2 Hz, 1H), 3.98 (t, *J* = 5.8 Hz, 2H), 2.46 (t, *J* = 7.1 Hz, 2H), 2.34 (s, 3H), 1.85-1.65 (m, 4H). ^{13}C {^{1}H} NMR (300 MHz, DMSO-d6, Figure S17) δ 157.3, 130.2, 129.1, 127.8, 127.8, 125.2, 117.0, 115.6, 114.6, 109.8, 109.7, 104.2, 67.3, 51.1, 28.1, 22.0, 9.7. HRMS *m/z* calculated for $C_{19}H_{20}NO_4S$ $[M–Cs]^-$: 358.1119, found 358.1128. IR (neat, cm $^{-1}$) 3413, 3310, 3064, 3048, 2931, 2860, 1675, 1611, 1535, 1515. Melting point (dec.): 226–232 °C.

Cesium 4-(4-(1-methyl-3-((1E,3E)-5-((Z)-1-methyl-2-(4-(4-sulfonatobutoxy)phenyl)-3H-indolizin-4-ium-3-ylidene)penta-1,3-dien-1-yl)indolizin-2-yl)phenoxy)butane-1-sulfonate (**SO_3C5**)**:** To a round bottom flask equipped with a stir bar was added 4-(4-(1-methylindolizin-2-yl)phenoxy)butane-1-sulfonate (**3**) (0.50 g, 1.02 mmol) to acetic anhydride (10.2 mL) followed by perchloric acid (0.088 mL, 1.02 mmol) and *N*-[5-(phenylamino)-2,4-pentadienylidene]aniline monohydrochloride (**4**) (0.15 g, 0.51 mmol). The mixture was then sonicated and stirred until all of the starting material appeared to have been consumed in this first phase of the reaction (about 10 minutes). When the starting material was no longer visible, the reaction was allowed to stir for another 10 minutes before the addition of triethylamine (0.17 mL, 1.22 mmol). The reaction mixture quickly turned green and was allowed to stir for 2 hours before diethyl ether was added to precipitate the crude product. The precipitate was filtered and rinsed once more with diethyl ether, collecting the solids. The solids were purified via reversed phase column chromatography beginning with 100% H_2O and gradually transitioning to 40:60 ethanol/H_2O. The water was removed by blowing air over the surface of the solution to avoid heating. The pure product was yielded as a dark green solid (250 mg, 53%). ^{1}H NMR (300 MHz, CD_3OD-d4, Figure S18) δ 8.89 (d, J = 6.8 Hz, 2H), 7.73 (d, J = 8.6 Hz, 2H), 7.66-7.54 (m, 4H), 7.42-7.22 (m, 7H), 7.12 (d, J = 8.5 Hz, 4H), 6.57 (t, J = 13.1 Hz, 2H), 4.16 (t, J = 5.9 Hz, 4H), 2.95 (t, J = 7.0 Hz, 4H), 2.20 (s, 6H), 2.14-1.94 (m, 8H). ^{13}C {^{1}H}NMR (300 MHz, CD_3OD-d4, Figure S19) δ 168.4, 160.9, 144.4, 140.1, 135.6, 132.6, 131.3, 129.7, 127.4, 126.2, 122.5, 121.2, 119.4, 118.0, 116.1, 68.9, 52.4, 29.5, 23.1, 9.3. HRMS *m/z* calculated for $C_{43}H_{44}CsN_2O_8S_2$ $[M+H]^+$: 913.1588, found 913.1606. IR (neat, cm $^{-1}$): 3375 (br), 3099, 3070, 3033, 2917, 2861, 1651, 1611, 1521, 1508. UV-Vis-NIR (DMSO) λ_{max} = 801 nm; UV-Vis-NIR (MeOH) λ_{max} = 791 nm; UV-Vis-NIR (H_2O) λ_{max} = 726 nm; UV-Vis-NIR (FBS) λ_{max} = 842 nm. Melting point (dec.): 211–217 °C.

Cesium (Z)-4-(4-(1-methyl-3-(3-(1-methyl-2-(4-(4-sulfonatobutoxy)phenyl)-3H-indolizin-4-ium-3-ylidene)-2-oxido-4-oxocyclobut-1-en-1-yl)indolizin-2-yl)phenoxy)butane-1-sulfonate (**SO_3SQ**): To a pressure flask equipped with a stir bar and was added methylindolizin-2-yl)phenoxy)butane-1-sulfonate (**3**) (0.100 g, 0.204 mmol) and 3,4-dihydroxy-1,2-cyclobutanedione (**5**) (0.012 g, 0.102 mmol). The reagents were dissolved in 10 mL methanol and degassed with N_2 for 10 minutes. The reaction mixture was then heated to 100 °C in an oil bath for 6 hours. The reaction mixture was then concentrated and the solids were further purified via reversed phase column chromatography beginning with 100% H_2O and gradually transitioning to

40:60 ethanol/H_2O. The water was removed by blowing air over the surface of the solution as the product appeared to be sensitive to heat. The pure product was yielded following this step as a metallic in appearance red solid (65 mg, 60%). ^{1}H NMR (300 MHz, CD_3OD-d4, Figure S20) δ 9.76 (d, *J* = 6.9 Hz, 2H), 7.57 (d, *J* = 8.7 Hz, 2H), 7.37 (dd, *J* = 6.8 Hz, 1.0 Hz, 2H), 7.23 (d, *J* = 8.6 Hz, 4H), 7.04-6.95 (m, 6H), 4.13 (t, *J* = 6.0 Hz, 4H), 2.95 (t, *J* = 7.0 Hz, 4H), 2.21 (s, 6H), 2.12-1.83 (m, 8H). ^{13}C {^{1}H} NMR (300 MHz, CD_3OD-d4, Figure S21) δ 177.8, 166.1, 160.1, 143.2, 138.6, 134.9, 132.9, 128.9, 127.7, 121.0, 119.5, 118.4, 116.1, 114.8, 68.7, 52.5, 29.6, 23.1, 9.5. HRMS *m/z* calculated for $C_{42}H_{39}N_2O_{10}S_2$ $[M–2Cs+2H]^–$: 795.2052, found 795.2050. IR (neat, cm $^{-1}$): 3398 (br), 3068, 3038, 2919, 2864, 1733, 1600, 1570, 1523. UV-Vis-NIR (DMSO) λ_{max} = 720 nm; UV-Vis-NIR (MeOH) λ_{max} = 704 nm; UV-Vis-NIR (H_2O) λ_{max} = 699 nm; UV-Vis-NIR (FBS) λ_{max} = 719 nm. Melting point: 240–244 °C.

Photostability Studies: All photostability studies were conducted at a concentration of 1×10^{-6} M to maintain consistency and deter any aggregative effects throughout the photodecomposition process. The samples were irradiated with a white LED lamp providing a spectral range from 400 nm – 1,100 nm. The experiment was allowed to take place under ambient conditions without any further precautions to remove oxygen from the system. UV-Vis-NIR was used to periodically measure the decline in absorption with respect to the λ_{max}. The photostability in methanol was conducted over a period of 24 hours while the photostability in water was conducted over a period of just 6 hours as the photodecomposition was observed within a shorter time frame.

Supporting Information

Photostability studies, electronic absorption studies, fluorescence studies, ^{1}H NMR and ^{13}C {^{1}H} NMR for the prepared compounds, and solubility studies.

Corresponding Authors

*J.H.D. e-mail: delcamp@olemiss.edu

Notes

The authors declare no competing financial interest.

Acknowledgements

The authors thank the National Science Foundation for Award 1757220.

References

(1) Luo, S.; Zhang, E.; Su, Y.; Cheng, T.; Shi, C. A Review of NIR Dyes in Cancer Targeting and Imaging. *Biomaterials* **2011**, *32*, 7127-7138.

(2) Li, X.; Gao, X.; Shi, W.; Ma, H. Design Strategies for Water-Soluble Small Molecular Chromogenic and Fluorogenic Probes. *Chem. Rev.* **2014**, *114*, 590-659.

(3) Guo, Z.; Park, S.; Yoon, J.; Shin, I. Recent Progress in the Development of Near-Infrared Fluorescent Probes for Bioimaging Applications. *Chem. Soc. Rev.* **2014**, *43*, 16-29.

(4) Jin, T. Review—Recent Progress in NIR Fluorophores Emitting over 1000 nm for Bioimaging. *ECS J. Solid State Sci. Technol.* **2019**, *8*, R9-R13.

(5) Zhu, S.; Tian, R.; Antaris, A. L.; Chen, X.; Dai, H. Near-Infrared-II Molecular Dyes for Cancer Imaging and Surgery. *Adv. Mater.* **2019**, *31*, 1900321.

(6) Wang, W.; Ma, Z.; Zhu, S.; Wan, H.; Yue, J.; Ma, H.; Ma, R.; Yang, Q.; Wang, Z.; Li, Q.; Qian, Y.; Yue, C.; Wang, Y.; Fan, L.; Zhong, Y.; Zhou, Y.; Gao, H.; Ruan, J.; Hu, Z.; Liang, Y.; Dai, H. Molecular Cancer Imaging in the Second Near-Infrared Window Using a Renal-Excreted NIR-II Fluorophore-Peptide Probe. *Adv. Mater.* **2018**, *30*, 1800106.

(7) Zhang, X. D.; Wang, H.; Antaris, A. L.; Li, L.; Diao, S.; Ma, R.; Nguyen, A.; Hong, G.; Ma, Z.; Wang, J.; Zhu, S.; Castellano, J. M.; Wyss-Coray, T.; Liang, Y.; Luo, J.; Dai, H. Traumatic Brain Injury Imaging in the Second Near-Infrared Window with a Molecular Fluorophore. *Adv. Mater.* **2016**, *28*, 6872-6879.

(8) Owens, E. A.; Henary, M.; El Fakhri, G.; Choi, H. S. Tissue-Specific Near-Infrared Fluorescence Imaging. *Acc. Chem. Res.* **2016**, *49*, 1731-1740.

(9) Detty, M. R.; Gibson, S. L.; Wagner, S. J. Current Clinical and Preclinical Photosensitizers for Use in Photodynamic Therapy. *J. Med. Chem.* **2004**, *47*, 3897-3915.

(10) Zhao, J.; Zhong, D.; Zhou, S. NIR-I-to-NIR-II Fluorescent Nanomaterials for Biomedical Imaging and Cancer Therapy. *J. Mater. Chem. B* **2018**, *6*, 349-365.

(11) Sun, X.; Zhuang, B.; Zhang, M.; Jiang, H.; Jin, Y. Intratumorally Injected Photothermal Agent-Loaded Photodynamic Nanocarriers for Ablation of Orthotopic Melanoma and Breast Cancer. *ACS Biomater. Sci. Eng.* **2019**, *5*, 724-739.

(12) Davies, K. S.; Linder, M. K.; Kryman, M. W.; Detty, M. R. Extended Rhodamine Photosensitizers for Photodynamic Therapy of Cancer Cells. *Bioorg. Med. Chem.* **2016**, *24*, 3908-3917.

(13) Suzuki, H. Organic Light-Emitting Materials and Devices for Optical Communicaiton Technology. *J. Photochem. Photobio. A* **2004**, *166*, 155-161.

(14) Hales, J. M.; Barlow, S.; Kim, H.; Mukhopadhyay, S.; Brédas, J.-L.; Perry, J. W.; Marder, S. R. Design of Organic Chromophores for All-Optical Signal Processing Applications. *Chem. Mater.* **2013**, *26*, 549-560.

(15) Samuel, I. D. W.; Turnbull, G. A. Organic Semiconductor Lasers. *Chem. Rev.* **2007**, *107*, 1272-1295.

(16) Tuong Ly, K.; Chen-Cheng, R.-W.; Lin, H.-W.; Shiau, Y.-J.; Liu, S.-H.; Chou, P.-T.; Tsao, C.-S.; Huang, Y.-C.; Chi, Y. Near-Infrared Organic Light-Emitting Diodes with Very High External Quantum Efficiency and Radiance. *Nat. Photon.* **2016**, *11*, 63-68.

(17) Ibrahim-Ouali, M.; Dumur, F. Recent Advances on Metal-Based Near-Infrared and Infrared Emitting OLEDs. *Molecules* **2019**, *24*, 1412.

(18) Qian, G.; Wang, Z. Y. Near-Infrared Organic Compounds and Emerging Applications. *Chem. Asian J.* **2010**, *5*, 1006-1029.

(19) Bricks, J. L.; Slominskii, Y. L.; Panas, I. D.; Demchenko, A. P. Fluorescent J-Aggregates of Cyanine Dyes: Basic Research and Applications Review. *Methods Appl. Fluoresc.* **2017**, *6*, 012001.

(20) Wang, J.; Lv, F.; Liu, L.; Ma, Y.; Wang, S. Strategies to Design Conjugated Polymer Based Materials for Biological Sensing and Imaging. *Coord. Chem. Rev.* **2018**, *354*, 135-154.

(21) Ilina, K.; MacCuaig, W.; Laramie, M.; Jeouty, J. N.; McNally, L. R.; Henary, M. Squaraine Dyes: Molecular Design for Different Applications and Remaining Challenges. *Bioconjug. Chem.* **2019**, DOI: 10.1021/acs.bioconjchem.9b00482.

(22) Yang, Z.; Sharma, A.; Qi, J.; Peng, X.; Lee, D. Y.; Hu, R.; Lin, D.; Qu, J.; Kim, J. S. Super-Resolution Fluorescent Materials: An Insight into Design and Bioimaging Applications. *Chem. Soc. Rev.* **2016**, *45*, 4651-4667.

(23) Smith, A. M.; Mancini, M. C.; Nie, S. Bioimaging: Second Window for in Vivo Imaging. *Nat. Nanotech.* **2009**, *4*, 710-711.

(24) Gao, F. P.; Lin, Y. X.; Li, L. L.; Liu, Y.; Mayerhoffer, U.; Spenst, P.; Su, J. G.; Li, J. Y.; Wurthner, F.; Wang, H. Supramolecular Adducts of Squaraine and Protein for Noninvasive Tumor Imaging and Photothermal Therapy in Vivo. *Biomaterials* **2014**, *35*, 1004-1014.

(25) Shindy, H. A. Fundamentals in the Chemistry of Cyanine Dyes: A Review. *Dyes and Pigm.* **2017**, *145*, 505-513.

(26) Escobedo, J. O.; Rusin, O.; Lim, S.; Strongin, R. M. NIR Dyes for Bioimaging Applications. *Curr. Opin. Chem. Biol.* **2010**, *14*, 64-70.

(27) Keereweer, S.; Van Driel, P. B. A. A.; Snoeks, T. J. A.; Kerrebijn, J. D. F.; Baatenburg de Jong, R. J.; Vahrmeijer, A. L.; Sterenborg, H. J. C. M.; Löwik, C. W. G. M. Optical Image-Guided Cancer Surgery: Challenges and Limitations. *Clin. Cancer Res.* **2013**, *19*, 3745-3754.

(28) Lerchenberger, M.; Gundogar, U.; Al Arabi, N.; Gallwas, J. K. S.; Stepp, H.; Hallfeldt, K. K. J.; Ladurner, R. Indocyanine Green Fluorescence Imaging During Partial Adrenalectomy. *Surg. Endosc.* **2019**, DOI: 10.1007/s00464-019-06985-7.

(29) McNamara, L. E.; Rill, T. A.; Huckaba, A. J.; Ganeshraj, V.; Gayton, J.; Nelson, R. A.; Sharpe, E. A.; Dass, A.; Hammer, N. I.; Delcamp, J. H. Indolizine-Squaraines: NIR Fluorescent Materials with Molecularly Engineered Stokes Shifts. *Chem. Eur. J.* **2017**, *23*, 12494-12501.

(30) Gayton, J.; Autry, S. A.; Meador, W.; Parkin, S. R.; Hill, G. A.; Hammer, N. I.; Delcamp, J. H. Indolizine-Cyanine Dyes: Near Infrared Emissive Cyanine Dyes with Increased Stokes Shifts. *J. Org. Chem.* **2019**, *84*, 687-697.

(31) Gayton, J. N.; Autry, S.; Fortenberry, R. C.; Hammer, N. I.; Delcamp, J. H. Counter Anion Effect on the Photophysical Properties of Emissive Indolizine-Cyanine Dyes in Solution and Solid State. *Molecules* **2018**, *23*, 3051.

(32) Rathnamalala, C. S. L.; Gayton, J. N.; Dorris, A. L.; Autry, S. A.; Meador, W.; Hammer, N. I.; Delcamp, J. H.; Scott, C. N. Donor-Acceptor-Donor NIR II Emissive Rhodindolizine Dye Synthesized by C-H Bond Functionalization. *J. Org. Chem.* **2019**, *84*, 13186-13193.

(33) Li, B.; Lu, L.; Zhao, M.; Lei, Z.; Zhang, F. An Efficient 1064 nm NIR-II Excitation Fluorescent Molecular Dye for Deep-Tissue High-Resolution Dynamic Bioimaging. *Angew. Chem. Int. Ed.* **2018**, *57*, 7483-7487.

(34) Antaris, A. L.; Chen, H.; Diao, S.; Ma, Z.; Zhang, Z.; Zhu, S.; Wang, J.; Lozano, A. X.; Fan, Q.; Chew, L.; Zhu, M.; Cheng, K.; Hong, X.; Dai, H.; Cheng, Z. A High Quantum Yield Molecule-Protein Complex Fluorophore for Near-Infrared II Imaging. *Nat. Commun.* **2017**, *8*, 15269.

(35) Rotermund, F.; Weigand, R.; Penzkofer, A. J-Aggregation and Disaggregation of Indocyanine Green in Water. *Chem. Phys.* **1997**, *220*, 385-392.

(36) Reindl, S.; Penzkofer, A.; Gong, S.-H.; Landthaler, M.; Szeimies, R. M.; Abels, C.; Bäumler, W. Quantum Yield of Triplet Formation for Indocyanine Green. *J. Photochem. Photobio. A* **1997**, *105*, 65-68.

(37) Zhang, Y.; Autry, S. A.; McNamara, L. E.; Nguyen, S. T.; Le, N.; Brogdon, P.; Watkins, D. L.; Hammer, N. I.; Delcamp, J. H. Near-Infrared Fluorescent Thienothiadiazole Dyes with Large Stokes Shifts and High Photostability. *J. Org. Chem.* **2017**, *82*, 5597-5606.

(38) Rüttger, F.; Mindt, S.; Golz, C.; Alcarazo, M.; John, M. Isomerization and Dimerization of Indocyanine Green and a Related Heptamethine Dye. *Eur. J. Org. Chem.* **2019**, *2019*, 4791-4796.